

# A PHENOMENOLOGICAL STUDY OF BFKL EVOLUTION \*

C. ROYON

*CEA, DAPNIA, Service de Physique des Particules,  
Centre d'Etudes de Saclay, France*

The QCD dipole picture allows to build an unified theoretical description -based on BFKL dynamics- of the total and diffractive nucleon structure functions measured at HERA. We use a four parameter fit to describe the 1994 H1 proton structure function  $F_2$  data in the low  $x$ , moderate  $Q^2$  range. The diffractive dissociation processes are discussed within the same framework, and a 6 parameter fit of the 1994 H1 diffractive structure function data is performed.

The BFKL dynamics can also be successfully tested at the  $e^+e^-$  collider LEP and a future high energy linear collider. The total  $\gamma^*\gamma^*$  cross-section is calculated in the Leading Order QCD dipole picture of BFKL dynamics, and compared with the one from 2-gluon exchange. Next to Leading order corrections to the BFKL evolution have been determined phenomenologically, and are found to give very large corrections to the BFKL cross-section, leading to a reduced sensitivity for observing BFKL effects. The  $Y$  dependence of the cross-section remains a powerful tool to increase the ratio between the BFKL and the 2-gluon cross-sections and is more sensitive to BFKL effects, even in the presence of large higher order corrections.

## 1 Description of the proton structure function $F_2$ in the BFKL framework

To obtain the proton structure function  $F_2$ , we use the  $k_T$  factorisation theorem, valid for QCD at high energy (small  $x$ ), in order to factorise the  $(\gamma g(k) \rightarrow q \bar{q})$  cross section and the unintegrated gluon distribution of a proton containing the physics of the BFKL pomeron <sup>1,2</sup>. The detailed calculations can be found in <sup>3</sup>.

We finally obtain:

$$F_2 \equiv F_T + F_L = \mathcal{N} a^{1/2} e^{(\alpha_{IP} - 1) \ln \frac{c}{x}} \frac{Q}{Q_0} e^{-\frac{a}{2} \ln^2 \frac{Q}{Q_0}} \quad (1)$$

where  $x$  and  $Q^2$  are respectively the momentum fraction of the interacting quark and the exchanged energy squared,  $\alpha_{IP} - 1 = \frac{4\bar{\alpha}N_c \ln 2}{\pi}$ , and  $a(x) = \left(\frac{\bar{\alpha}N_c}{\pi} 7\zeta(3) \ln \frac{c}{x}\right)^{-1}$ . The free parameters for the fit of the H1 data are  $\mathcal{N}$ , the normalisation,  $\alpha_{IP}$ , the pomeron intercept,  $Q_0$ , and  $c$ .

In order to test the accuracy of the  $F_2$  parametrisation obtained in formula (1), a fit using the recently published data from the H1 experiment <sup>4</sup> has been performed <sup>3</sup>. We have only used the points with  $Q^2 \leq 150 \text{GeV}^2$  to remain in a reasonable domain of validity of the QCD dipole model. The  $\chi^2$  is 88.7 for 130 points, and the values of the parameters are  $Q_0 = 0.522 \text{GeV}$ ,  $\mathcal{N} = 0.059$ , and  $c = 1.750$ , while  $\alpha_{IP} = 0.282$ . Commenting on the parameters, let us note that the effective coupling constant extracted using (3) from  $\alpha_{IP}$  is  $\alpha = 0.11$ , close to  $\alpha(M_Z)$  used in the H1 QCD fit. It is an acceptable value for the small fixed value of the coupling constant required by the BFKL framework. The running of the coupling constant is not

---

\*INVITED TALK GIVEN AT THE HADRON 13 CONFERENCE, MUMBAI, 13-20 JANUARY 1999

taken into account in the present BFKL scheme. This could explain the rather low value of the effective  $\alpha_{IP}$  which is expected to be decreased by the next leading corrections. The value of  $Q_0$  corresponds to a transverse size of 0.4 fm which is in the correct range for a proton non-perturbative characteristic scale. The value of  $\mathcal{N}$  determines the amount of primordial dipoles in the proton to be

$$\omega(1/2) = \mathcal{N} \frac{128}{11\pi \alpha^2 N_c e_f^2} \sqrt{\frac{\pi}{2}} \simeq 7.55/e_f^2,$$

The parameter  $c$  sets the “time” scale for the formation of the interacting dipoles. It defines the effective total rapidity interval which is  $\log(1/x) + \log c$ , the constant being not predictable (but of order 1) at the leading logarithmic approximation.

## 2 Diffractive structure functions

In the dipole approach, two components contribute to the diffractive structure function. First, the elastic component corresponds to the elastic interaction of two dipole configurations. It is expected to be dominant in the finite  $\beta$  region, i.e. for small relative masses of the diffractive system. Second, there is an inelastic component where the initial photon dipole configuration is diffractively dissociated in multi-dipole states by the target. This process is expected to be important at small  $\beta$  (large masses).

The expressions for the elastic component is the following:

$$F_T^{D(el)} = 12 \frac{N_c e^2 \alpha_s^4}{\pi} x_{IP}^{-2\alpha_{IP}+1} a^3(x_{IP}) \log^3 \frac{Q}{2Q_0 \sqrt{\beta}} e^{-a(x_{IP}) \log^2 \frac{Q}{2Q_0 \sqrt{\beta}}} \quad (2)$$

$$\times \beta(1-\beta) \left[ {}_2F_1 \left( -\frac{1}{2}, \frac{3}{2}; 2; 1-\beta \right) \right]^2, \quad (3)$$

$$F_L^{D(el)} = 16 \frac{N_c e^2 \alpha_s^4}{\pi} x_{IP}^{-2\alpha_{IP}+1} a^3(x_{IP}) \log^2 \frac{Q}{2Q_0 \sqrt{\beta}} e^{-a(x_{IP}) \log^2 \frac{Q}{2Q_0 \sqrt{\beta}}} \quad (4)$$

$$\times \beta^2 \left[ {}_2F_1 \left( -\frac{1}{2}, \frac{3}{2}; 1; 1-\beta \right) \right]^2, \quad (5)$$

with  $\alpha_{IP}$ , and  $a(x_{IP})$  defined in the first section. The inelastic component reads:

$$F_{T,L}^{D(in)} = 2^9 \sqrt{\frac{2}{\pi}} H_{T,L} \left( \frac{1}{2} \right) \frac{N_c e^2 \alpha_s^5}{\pi^4} x_{IP}^{-2\alpha_{IP}+1} a^3(x_{IP}) \frac{Q}{Q_0} e^{-\frac{a(\beta)}{2} \log^2 \frac{Q}{4Q_0}} a^{\frac{1}{2}}(\beta) \beta^{1-\alpha_{Pom}}. \quad (6)$$

With this model, we are ready to write a full parametrization adequate for the description of the data. The free parameters of the dipole model are  $\alpha_{IP}$ , which is related to the fixed coupling constant  $\alpha_s$  in the BFKL scheme at leading order,  $Q_0$ , corresponding to a non-perturbative scale for the proton, and the three normalizations  $N_T^{(el)}$ ,  $N_L^{(el)}$ ,  $N^{(in)}$ . As it is now well-known, a secondary trajectory based on reggeon exchange is added in order to take into account the large-mass and small rapidity gap domain. Reggeon exchange can here be simply parametrized in the following way:  $F_2^{D(R)}(x_P, \beta, Q^2) = f^R(x_P) F_2^R(\beta, Q^2)$ , where the reggeon

flux  $f^R(x_P)$  is assumed to follow a Regge behaviour with a linear trajectory  $\alpha_R(t) = \alpha_R(0) + \alpha'_R t$ :  $f^R(x_P) = \int_{t_{cut}}^{t_{min}} dt \frac{e^{B^R t}}{x_P^{2\alpha_R(t)-1}}$ , where  $|t_{min}|$  is the minimum kinematically allowed value of  $|t|$  and  $t_{cut} = -1$  GeV $^2$  is the limit of the measurement. The values of  $B^R$  and  $\alpha'_R$  are fixed with data from hadron-hadron collisions<sup>5</sup>. The reggeon structure function is assumed to be the pion structure function<sup>6</sup>. The free parameters for this component are the reggeon normalisation  $N^R$  and exponent  $\alpha_R$ .

A fit to the recently published H1<sup>5</sup> and ZEUS<sup>7</sup> diffractive structure function data is performed separately. The result of the H1 fit is shown in Figure 1. The fit to the H1 data leads to a very good  $\chi^2$  (1.17 per degree of freedom with statistical errors only). The parameters and the features of the fits are given in detail in Ref. <sup>8</sup>, and we will comment here only on the main parameters. The value of  $\alpha_R$  ( $\alpha_R=0.68$ ) is consistent with the usual values found for secondary reggeon contributions if interference effects are not taken into account<sup>5</sup>. The value of  $\alpha_P$  ( $\alpha_P=1.40$ ) is found to be consistent with the expected intercept for a hard BFKL pomeron<sup>2</sup>. This intercept is higher than the value obtained from the fit to the structure function  $F_2$ .  $Q_0$  ( $Q_0=0.43$ ) is a typical non perturbative scale for the proton and very close to the value obtained in the proton structure function fit. It should be noted that the scale  $Q_0$  appears in a quite non trivial way as the virtuality in the inelastic component ( $Q/4Q_0$ ), and in the elastic one ( $Q/2\sqrt{\beta}Q_0$ ).

The fit to the ZEUS data leads to a worse  $\chi^2$  ( $\chi^2/dof = 1.95$  with statistical errors only). In order to investigate the origin of these differences, a direct comparison between ZEUS and H1 data has been performed<sup>8</sup>. The H1 data have been interpolated to the ZEUS closest bins in  $\beta$  and  $Q^2$  using the dipole model fit. This interpolation is weakly sensitive to the model used as the interpolation in the kinematical variables is very small. It was checked that the use of the model by Bartels et al.<sup>9</sup> gives a similar result. The striking feature is that the main difference between the H1 and ZEUS fits comes from the region where the data are different, showing that this region influences the global fit.

Let us now comment about some of the main features of the fit. Some additional details and discussions can be found in<sup>8</sup>. First, the effective intercept of the proton diffractive structure function in the QCD dipole picture is clearly not consistent with the soft pomeron value (1.08), but much lower than the bare pomeron intercept obtained in the fit ( $\alpha_P = 1.40$ ). This can be explained by the large logarithmic corrections induced by the  $a^3(x_P)$  term, proportional to  $\log^3(1/x_P)$ , present in both diffractive components (see formulae 3, 5, 6). The effect of this logarithmic term induces also an  $x_P$  dependence of the intercept. Moreover, the  $x_P$  dependence of the intercept is different between the elastic and the inelastic components. This induces a breaking of factorisation directly for the diffractive components of this model, which comes in addition to the known factorisation breaking due to secondary trajectories.

One interesting feature of the diffractive proton structure functions was the  $Q^2$  dependence at fixed  $x_P$  as a function of  $\beta$  as was pointed out experimentally by the H1 collaboration<sup>5</sup> and confirmed at lower  $Q^2$ . In the QCD dipole model, this experimental feature is described by a non trivial interplay between the two

diffractive components. In Figure 2, the dipole fit is compared with the H1 result showing the contribution of each component: at small  $\beta$ , the inelastic component dominates and varies quasi linearly in  $\log Q^2$ , and at high  $\beta$ , this component is depressed similarly to the total structure function, but is progressively substituted by the elastic component.

One important result of the dipole model is also the fact that the longitudinal elastic component is found to be high at high  $\beta$ , which leads to high values of the ratio  $R$  of the longitudinal to the transverse components at high values of  $\beta$ . We obtain that the  $R$  ratio remains small ( $\sim 0.2$ ) in almost the full kinematical plane except notably at high  $\beta$  where it may reach high values such as 2. Note that this value is in the range of the measured  $R$  ratio with vector meson production. A measurement of  $R$  in diffraction would thus be of great interest and would be a good test of the model. It is instructive to notice that another model of diffraction based on selecting  $q\bar{q}$  and  $q\bar{q}g$  components of the photon <sup>9</sup> also leads to a large contribution of the longitudinal  $q\bar{q}$  contribution at high  $\beta$ .

### 3 $\gamma^*\gamma^*$ total cross-section

Here, we want to calculate the total  $\gamma^*\gamma^*$  cross-section derived in the Leading Order QCD dipole picture of BFKL dynamics. This could be a good test of the BFKL equation which can be performed at  $e^+e^-$  colliders (LEP or linear collider LC). The advantage of this process compared to the ones discussed in the previous sections is that it is a purely perturbative process.

In this study, we compare the 2-gluon and the BFKL cross-sections. Defining  $y_1$  (resp.  $y_2$ ), and  $Q_1^2$  (resp.  $Q_2^2$ ) to be the rapidities and the squared transferred energies for both virtual photons, one gets

$$d\sigma_{e^+e^-}(Q_1^2, Q_2^2; y_1, y_2) = \frac{4}{9} \left( \frac{\alpha_{e.m}^2}{16} \right)^2 \alpha_s^2 \pi^2 \sqrt{\pi} \frac{dQ_1^2}{Q_1^2} \frac{dQ_2^2}{Q_2^2} \frac{dy_1}{y_1} \frac{dy_2}{y_2} \frac{1}{Q_1 Q_2} \\ \frac{4\alpha_s N_c}{\sqrt{\frac{14\alpha_s N_c}{\pi} Y \zeta(3)}} \frac{Y \ln 2}{\pi} \times e^{-\frac{\ln^2 \frac{Q_1^2}{Q_2^2}}{\frac{56\alpha_s N_c}{\pi} Y \zeta(3)}} [2l_1 + 9t_1] [2l_2 + 9t_2], \quad (7)$$

for the BFKL-LO cross-section, where  $t_1 = \frac{1+(1-y_1)^2}{2}$ ,  $l_1 = 1 - y_1$ , and an analogous definition for  $t_2$  and  $l_2$ , and  $Y = \ln \frac{sy_1 y_2}{\sqrt{Q_1^2 Q_2^2}}$ . The 2-gluon cross-section has been calculated exactly within the high energy approximation (NNNLO calculation) and reads

$$d\sigma_{e^+e^-}(Q_1^2, Q_2^2; y_1, y_2) = \frac{dQ_1^2}{Q_1^2} \frac{dQ_2^2}{Q_2^2} \frac{dy_1}{y_1} \frac{dy_2}{y_2} \frac{64(\alpha_{e.m}^2 \alpha_s)^2}{243\pi^3} \frac{1}{Q_1^2} \\ \left[ t_1 t_2 \ln^3 \frac{Q_1^2}{Q_2^2} + (7t_1 t_2 + 3t_1 l_2 + 3t_2 l_1) \ln^2 \frac{Q_1^2}{Q_2^2} \right. \\ \left. + \left( \frac{119}{2} - 2\pi^2 \right) t_1 t_2 + 5(t_1 l_2 + t_2 l_1) + 6l_1 l_2 \right] \ln \frac{Q_1^2}{Q_2^2}$$

$$+ \left( \frac{1063}{9} - \frac{14}{3}\pi^2 \right) t_1 t_2 + (46 - 2\pi^2)(t_1 l_2 + t_2 l_1) - 4l_1 l_2 \right]. \quad (8)$$

Results based on the calculations developed above will be given for LEP (190 GeV centre-of-mass energy) and a future Linear Collider (500 - 1000 GeV centre-of-mass energy).  $\gamma^* \gamma^*$  interactions are selected at  $e^+ e^-$  colliders by detecting the scattered electrons, which leave the beampipe, in forward calorimeters. Presently at LEP these detectors can measure electrons with an angle  $\theta_{tag}$  down to approximately 30 mrad. For the LC it has been argued <sup>10</sup> that angles as low as 20 mrad should be reached. Presently angles down to 40 mrad are foreseen to be instrumented for a generic detector at the LC.

Let us first specify the region of validity for the parameters controlling the basic assumptions made in the previous chapter. The main constraints are required by the validity of the perturbative calculations. The “perturbative” constraints are imposed by considering only photon virtualities  $Q_1^2, Q_2^2$  high enough so that the scale  $\mu^2$  in  $\alpha_S$  is greater than 3 GeV<sup>2</sup>.  $\mu^2$  is defined using the Brodsky Lepage Mackenzie (BLM) scheme <sup>11</sup>,  $\mu^2 = \exp(-\frac{5}{3})\sqrt{Q_1^2 Q_2^2}$  <sup>11</sup>. In this case  $\alpha_S$  remains always small enough such that the perturbative calculation is valid. In order that gluon contributions dominates the QED one,  $Y$  is required to stay larger than  $\ln(\kappa)$  with  $\kappa = 100$ . (see Ref. <sup>11</sup> for discussion). Furthermore, in order to suppress DGLAP evolution, while maintaining BFKL evolution will constrain  $0.5 < Q_1^2/Q_2^2 < 2$  for all nominal calculations. The comparison between the DGLAP-DLL and the 2-gluon cross-section in the LO approximation shows that both cross-sections are similar when  $Q_1$  and  $Q_2$  are not too different ( $0.5 < Q_1^2/Q_2^2 < 2$ ), so precisely in the kinematical domain where the BFKL cross-section is expected to dominate. However, when  $Q_1^2/Q_2^2$  is further away from one, the LO 2-gluon cross-section is lower than the DGLAP one, especially at large  $Y$ . This suggests that the 2-gluon cross-section could be a good approximation of the DGLAP one if both are calculated at NNNLO and restricted to the region where  $Q_1^2/Q_2^2$  is close to one. In this paper we will use the exact NNNLO 2-gluon cross-section in the following to evaluate the effect of the non-BFKL background, since the 2-gluon term appears to constitute the dominant part of the DGLAP cross-section in the region  $0.5 < Q_1^2/Q_2^2 < 2$ .

We will not discuss here all the phenomenological results, and some detail can be found in <sup>12</sup>, as well as the detailed calculations. We first study the effect of the tagged electron energy and angle. We first study the effect of increasing the LC detector acceptance for electrons scattered under small angles and the ratio of the 2-gluon and the BFKL-LO cross-sections increase by more a factor 3 if the tagging angle varies between 40 and 20 mrad. The effect of lowering the tagging energy is smaller. An important issue on the BFKL cross-section is the importance of the NLO corrections and we adopt a phenomenological approach to estimate the effects of higher orders. First, at Leading Order, the rapidity  $Y$  is not uniquely defined, and we can add an additive constant to  $Y$ . This corresponds to the  $c$  parameter we discussed in the first section. A second effect of NLO corrections is to lower the value of the so called Lipatov exponent in formula 7. In the same  $F_2$  fit described in section 1, the value of the Lipatov exponent  $\alpha_{PL}$  was fitted and found to be 1.282, which gives an effective value of  $\alpha_s$  of about 0.11. The same idea can be applied phenomenologically for the  $\gamma^* \gamma^*$  cross-section. For this purpose,

	$\text{BFKL}_{LO}$	$\text{BFKL}_{NLO}$	2-gluon	ratio
LEP	0.57	3.1E-2	1.35E-2	2.3
LEP*	3.9	0.18	6.8E-2	2.6
LC 40 mrad	6.2E-2	6.2E-3	2.64E-3	2.3
LC 20 mrad	3.3	0.11	3.97E-2	2.8

Table 1. Final cross-sections (pb), for selections described in the text.

$Y$ cut	$\text{BFKL}_{NLO}$	2-gluon	ratio
no cut	1.1E-2	3.97E-2	2.8
$Y \geq 6.$	5.34E-2	1.63E-2	3.3
$Y \geq 7.$	2.54E-2	6.58E-3	3.9
$Y \geq 8.$	6.65E-3	1.43E-3	4.7
$Y \geq 8.5$	1.67E-3	3.25E-4	5.1
$Y \geq 9.$	5.36E-5	9.25E-6	5.8

Table 2. Final cross-sections (pb), for selections described in the text, after different cuts on  $Y$

we modify the scale in  $\alpha_S$  so that the effective value of  $\alpha_S$  for  $Q_1^2 = Q_2^2 = 25$  GeV $^2$  is about 0.11. Finally, the results of the BFKL and 2-gluon cross-sections are given in Table 1 if we assume both effects. The ratio BFKL to 2-gluon cross-sections is reduced to 2.3 if both effects are taken into account together. In the same table, we also give these effects for LEP with the nominal selection and at the LC with a detector with increased angular acceptance. The column labelled 'LEP\*' gives the results for the kinematic cuts used by the L3-collaboration who have recently presented preliminary results <sup>13</sup>. The cuts are  $E_{tag} = 30$  GeV and  $\theta_{tag} > 30$  mrad and  $\mu^2 > 2$  GeV $^2$ . For this selected region the difference between NLO-BFKL and 2-gluon cross-section is only a factor of 2.4. A cut on  $Q_1^2/Q_2^2$ , as done for the other calculations in this paper, would help to allow a more precise determination of the 2-gluon 'background'. Another idea to establish the BFKL effects in data is to study the energy or  $Y$  dependence of the cross-sections, rather than the comparison with total cross-sections itself. To illustrate this point, we calculated the BFKL-NLO and the 2-gluon cross-sections, as well as their ratio, for given cuts on rapidity  $Y$  (see table 2). We note that we can reach up to a factor 5 difference ( $Y \geq 8.5$ ) keeping a cross-section measurable at LC. The cut  $Y \geq 9.$  would give a cross-section hardly measurable at LC, even with the high luminosity possible at this collider. Cuts on  $Y$  will be hardly feasible at LEP because of the low cross-sections obtained already without any cuts on  $Y$ .

#### 4 Conclusion

Finally the colour dipole model formalism calls for a unified description of the diffractive and total deep-inelastic scattering events. We showed that within the precision of the current data, there are quite a few indications (similar scale  $Q_0$ ,

softening of the hard Pomeron by logarithmic factors in diffraction,etc...) of such a common theoretical ground. However, further tests of the model are deserving. The first one would be a confrontation of the predicted  $R$  ratio with the data if available: indeed, the various models should predict quite different contributions from the two polarization states of the photon. Other useful tests concern the final states. For instance one can compute the predictions for diffractive vector meson production and confront them to the recent data. Such tests might help distinguish between the few different models for hard diffraction which are able to describe the data.

The other topic discussed here is the difference between the 2-gluon and BFKL  $\gamma^*\gamma^*$  cross-sections both at LEP and LC. The LO BFKL cross-section is much larger than the 2-gluon cross-section. Unfortunately, the higher order corrections of the BFKL equation (which we estimated phenomenologically) are large, and the 2-gluon and BFKL-NLO cross-sections ratios are reduced to a factor two to four. The  $Y$  dependence of the cross-section remains a powerful tool to increase this ratio and is more sensitive to BFKL effects, even in the presence of large higher order corrections. Further more, the higher order corrections to the BFKL equations were treated here only phenomenologically, and we noticed that even a small change on the BFKL pomeron intercept implies large changes on the cross-sections. The uncertainty on the BFKL cross-section after higher order corrections is thus quite large. We thus think that the measurement performed at LEP or at LC should be compared to the precise calculation of the 2-gluon cross-section after the kinematical cuts described in this paper, and the difference can be interpreted as BFKL effects. A fit of these cross-sections will then be a way to determine the BFKL pomeron intercept after higher order corrections.

## 5 Acknowledgements

The results described in the present contribution come from a fruitful collaboration with A.Bialas, M.Boonekamp, S.Munier, H.Navelet, R.Peschanski, A.De Roeck, S.Wallon. I also thank the organisers for financial support.

## References

1. A. H. Mueller, *Nucl. Phys.* **B415** (1994) 373, A. H. Mueller, B. Patel, *Nucl. Phys.* **B425** (1994) 471, A. H. Mueller, *Nucl. Phys.* **B437** (1995) 107.
2. V. S. Fadin, E.A. Kuraev and L.N. Lipatov, *Phys. Lett.* **B60** (1975) 50; I. I. Balitsky and L.N. Lipatov, *Sov. J. Nucl. Phys.* **28** (1978) 822.
3. H. Navelet, R. Peschanski, Ch. Royon, S. Wallon, *Phys. Lett.* **B385** (1996) 357, H.Navelet, R.Peschanski, Ch.Royon, *Phys.Lett.*, **B366**, (1996) 329.
4. H1 coll., *Nucl.Phys. B470* (1996) 3
5. C. Adloff et al., H1 coll., *Z.Phys.* **C76** (1997) 613.
6. M.Glück, E.Reya, A.Vogt, *Z.Phys.* **C53** (1992) 651.
7. J. Breitweg, ZEUS coll., *Eur. Phys. J.* **C1** (1998) 81.
8. A. Bialas, R. Peschanski, Ch. Royon, *Phys. Rev.* **D57** (1998) 6899, S.Munier, R.Peschanski, Ch.Royon, *Nucl.Phys.* **B534** (1998) 297.

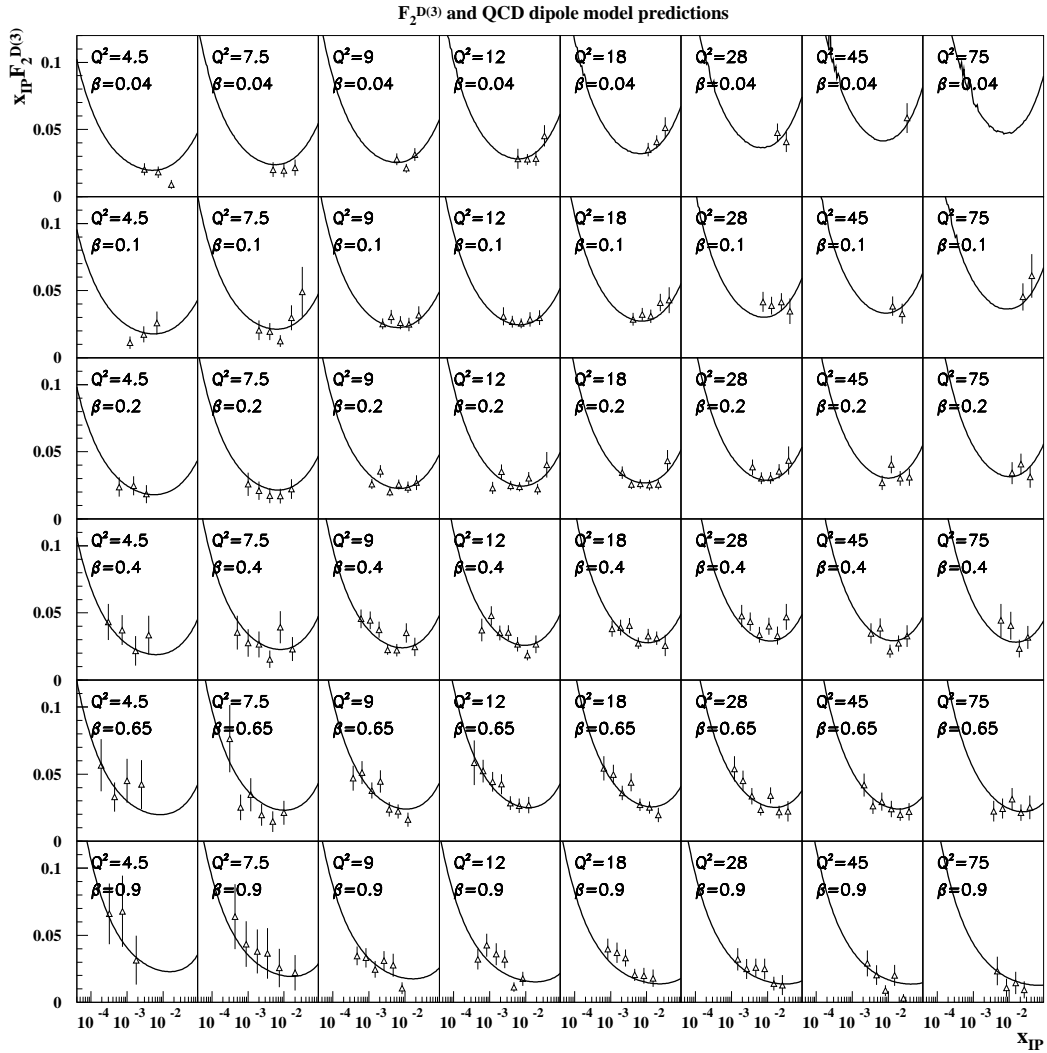


Figure 1. Result of the  $F_2^D$  fit to the H1 data. The data are displayed by triangles (with statistical and systematic errors added in quadrature) as a function of  $x_{IP}$  in  $\beta$  and  $Q^2$  bins. The fit has been performed with statistical errors only and is displayed in full line.

9. J. Bartels, J. Ellis, H. Kowalski, M. Wüsthoff, *Eur.Phys.J.* **C7** (1999) 443, J.Bartels, C.Royon, preprint DESY 98-152, [hep-ph/9809344](#).
10. J. Bartels, A. De Roeck and H. Lotter, *Phys. Lett.* **B389** (1996) 742-748, J. Bartels, A. De Roeck and H. Lotter, C. Ewerz, DESY preprint 97-123E, [hep-ph/9710500](#).

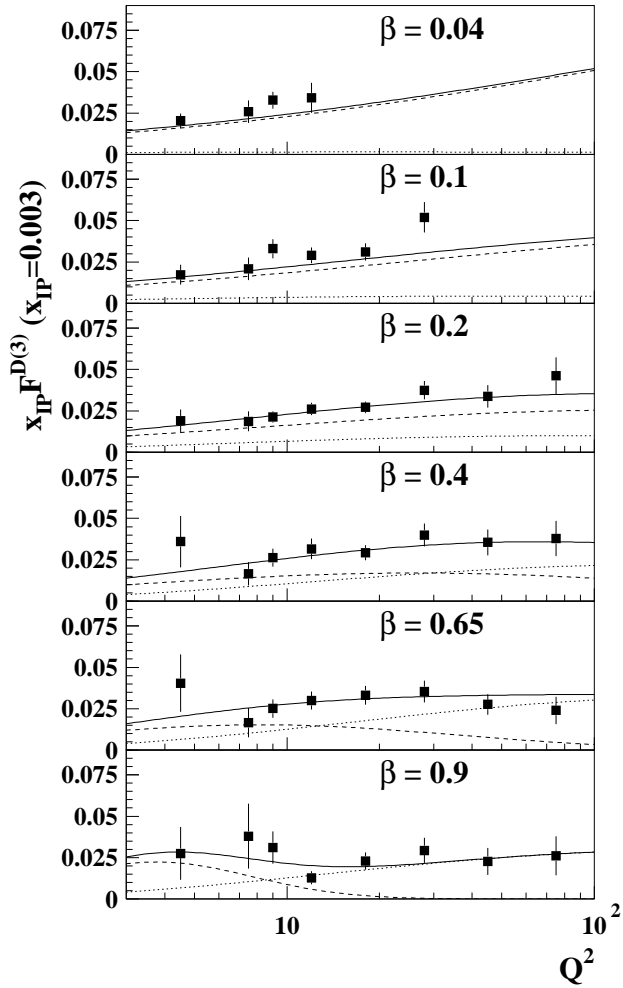


Figure 2. Scaling violations. The dependence of  $x_{IP} F_2^D$  on  $Q^2$  for different values of  $\beta$  at fixed  $x_{IP}$  ( $3.10^{-3}$ ) is shown together with the dipole model fit. Dotted line: elastic component, dashed line: inelastic component, full line: total.

11. S.J. Brodsky, F. Hautmann and D.E. Soper, Phys. Rev. Lett. **78** (1997) 803-806, Phys. Rev. **D56** (1997) 6957-6979, G.P. Lepage, P.B. Mackenzie, Phys. Rev. **D48** (1993) 2250, S.J. Brodsky, G.P. Lepage, P.B. Mackenzie, Phys. Rev. **D28** (1983) 228.
12. M.Boonekamp, A. De Roeck, Ch. Royon, S.Wallon, preprint DAPNIA-SPP 99-01, [hep-ph/9812523](https://arxiv.org/abs/hep-ph/9812523).
13. Chu Lin, contributed talk at HADRON98, Stara Lesna, September 1998;

M. Kienzle, contributed talk at the 2-photon workshop, Lund, September 1998.